actuators

MDPI

Article

A Study of a Bistable Reciprocating Piston Pump Driven by Shape Memory Alloys and Recuperative Springs

Mihail Kostov [1], Todor Todorov [1], Rosen Mitrev [2,*], Konstantin Kamberov [3] and Rumen Nikolov [4]

[1] Department of Theory of Mechanisms and Machines, Faculty of Industrial Technology, Technical University of Sofia, 1797 Sofia, Bulgaria
[2] Department of Logistics Engineering, Material Handling and Construction Machines, Mechanical Engineering Faculty, Technical University of Sofia, 1797 Sofia, Bulgaria
[3] Department of Technology of Machine Tools and Manufacturing, Technical University of Sofia, 1797 Sofia, Bulgaria
[4] Department of Precision Engineering and Measurement Instruments, Technical University of Sofia, 1797 Sofia, Bulgaria
* Correspondence: rosenm@tu-sofia.bg

Abstract: This paper presents and examines a new design concept for a bistable reciprocating piston pump. The bistable pump mechanism belongs to the bistable mechanisms, which have two stable positions at the end of the suction and discharge strokes. The transition between the stable positions is achieved by using triggering force at each beginning of suction and discharge and subsequent movement using a recuperative spring. In this mechanism, the triggering forces are created by two Shape Memory Alloy (SMA) wires. Geometric and force expressions for the pump suction and discharge strokes are derived. Additional equations are obtained for the balance of moments for the two stable equilibrium positions and the unstable position in the middle of the stroke. Numerical studies have been conducted for the suction and discharge strokes, considering the force exerted by the gas on the piston, which is modelled by an indicator diagram assuming a polytropic process. It was found that the load on the mechanism has significant non-uniformity. The diagrams illustrating the distribution of total moments showed that the cold SMA wire shifted the point of instability. The numerical example shows how to choose the right spring stiffness to obtain energy recovery. In this way, the triggering SMA forces act only at the beginning of the two strokes and, after that, the recuperative forces substitute the action of the SMA forces. The theoretical relationships and methods presented here are suitable for synthesizing new pumps or analyzing similar mechanisms.

Keywords: bistable mechanism; shape memory alloys; reciprocating pump; recuperation

Citation: Kostov, M.; Todorov, T.; Mitrev, R.; Kamberov, K.; Nikolov, R. A Study of a Bistable Reciprocating Piston Pump Driven by Shape Memory Alloys and Recuperative Springs. *Actuators* **2023**, *12*, 90. https://doi.org/10.3390/act12020090

Academic Editor: Hongli Ji

Received: 28 January 2023
Revised: 11 February 2023
Accepted: 15 February 2023
Published: 17 February 2023

1. Introduction

Over the last two decades, the increase in industrial production and the availability of SMA (Shape Memory Alloy) components have made it possible to create many innovative mechatronic devices with specific functionalities. Two well-studied SMA properties are primarily used—Shape Memory and superelasticity effects [1–3]. Both properties arise from the reversible change of the crystal structure of SMA under the influence of temperature or mechanical stresses. From a mechanical viewpoint, the Shape Memory Effect manifests as an effect in which, after heating, a plastically deformed structural element recovers its original shape and size. In the superelasticity effect, for a constant temperature above the austenitic finish temperature and the external load applied, the element undergoes a large deformation, which is reversible when the load is removed. These properties allow the creation of devices with various functionalities using a minimum amount of building parts. In the available literature, special attention was given to SMA applications to build mechanisms with two stable positions, called bistable mechanisms.

The SMA elements generate forces that switch the system between the two positions. The bistable mechanism keeps its stable position locked in one of two possible positions until a force with the required magnitude and direction is applied to switch it to the other stable position. Another feature of these mechanisms is that when switching to the other stable position, the potential energy accumulated in the elastic elements forces the mechanism to pass through the unstable equilibrium position quickly.

Bistable mechanisms combined with SMA elements have attracted research attention and have been used to create numerous devices. The study of a crawling robot actuated by two antagonistic SMA springs was described in [4], and in [5], a method for analyzing and designing SMA-actuated compliant bistable mechanisms was presented. The authors of [6] developed an innovative, compliant industrial gripper powered by a bistable SMA actuator with low mass. The paper [7] presented a novel design of an energy-efficient, adaptive material-handling system containing a bistable SMA-actuated vacuum suction cup, which can replace the pneumatic grippers widely used in the industry. The authors of [8] described an interesting electromechanical device composed of a nitinol wire and a bias spring, which implements binary logical functions using a bistable effect.

SMA-controlled bistable mechanisms are often combined with other drive principles to extend functionality. The authors of [9] studied a new microactuator design with high blocking forces, using two actuation principles simultaneously by combining SMA microactuators with electroplated magnetic layers placed in an external magnetic field, which achieved better device functionality. Another paper [10] presented a compound actuator that combined the advantages of SMA and piezoelectric materials for changing the deformation of a cantilever beam made of asymmetric composite. The main benefit was that it could perform bi-directional control and achieve two stable beam states.

Using SMA elements has the following additional advantages: they are actuators with high energy density compared to other driving principles [11], they have self-sensing capabilities [12] and great potential for miniaturization [13,14], but their accurate control when following trajectories is limited [15,16]. Other limiting factors are low operating frequency [14,17] and long response time [18].

In addition to experimenting with physical models of bistable mechanisms, theoretical studies are conducted at a smaller scale. The main reason for this is that SMAs shows a complex nonlinear behaviour combined with temperature hysteresis described by multiple parameters that vary widely [19]. The authors of [20] developed a complex theoretical model describing the thermomechanical behaviour of a controllable bistable beam utilizing a nonlinear dynamic model. A further difficulty is that these devices combine multiple interacting physical domains, described by complex systems of coupled non-linear differential equations. Some authors overcame these theoretical difficulties by numerical simulation. The authors of [21] used finite element analysis to overcome the mathematical difficulties in stress modelling in a self-switching buckled beam. The approach presented in [22] is similar in modelling bistable mechanisms with elastic links used in space applications. A novel application of the bistable mechanisms is their use in fluid valves [23,24]. The authors patented the valve actuator [25,26] which also utilized a bistable mechanism operated by SMA wires.

Bistable mechanisms are also very suitable for pumps. The patent [27] presented a design of a pump where a bistable mechanism was applied to control the rate of a liquid in a pump in which pump capacity was stable at either the upper limit or the lower limit of the variable capacity range depending on the switching state. A bistable auxiliary device was applied in [28] as a flip-flop. A linear series of bistable overlapping shallow domes formed into a metal strip were used in the flex-actuated bistable dome pump [29]. A head of a bistable compressor with an additional compression chamber and a pressure relief valve were applied in [30]. A novel compressor design based on the bistable effect combined with SMA driving elements was presented in [31].

The motivation for the present work is the potential possibility to obtain an energy-efficient pump through a combination of SMA with a bistable mechanism. The pump is

expected to be efficient because the driving forces generated by the SMA wires are applied only at the beginning of the movement, after which the elements of the mechanism move under the action of recuperative springs.

This paper aims to introduce a new design concept for a bistable pump with a recuperative spring powered by SMA wires. The bistable pump design was based on an upgrade of the operating principle of the author's patented fluid valve [26] towards adding a lever system and a piston to convert it to a pump. It also aims to develop a theoretical method for synthesizing such a pump and prove its operability.

Furthermore, this document is structured in the following way. Section 2 details the design and operation of the pump under study. In Section 3, geometric and force relationships are derived for the considered mechanism. Section 4 is devoted to numerical studies and discussions. Section 5 presents experimental studies of a similar system. The research findings are presented in Section 6.

2. Design Concept of the Developed Reciprocating Piston Pump with Bistable Action Driven by Recuperative Springs

The authors' design concept and operating principle of the pump are illustrated in Figure 1 [31]. A rocker 1, consisting of three undeformable rigidly connected arms *OA*, *OB*, and *OC*, rotates about the revolute joint *O* with respect to the pump housing 0. The coupler 2 is connected by a revolute joint in point *B* to the rocker 1 and to the second revolute joint in point *D* to the piston 3. An extension piston spring 4 is connected to the revolute joint *B* and the housing in point *E*. The compression recuperative spring 5 is connected to point *C* of the rocker 1 and to point *F* of housing 1. The SMA wire 6, named "suction SMA wire", is mounted between point *M* of the rocker 1 and point *N* of housing 0. A second SMA wire 7, named "discharge SMA wire", connects the rocker 1 in point *A* to the housing in point *K*. The piston 3 slides in the cylinder 8 belonging to housing 0. On the bottom side of cylinder 8, there are a suction valve 9 and a discharge valve 10. The rotation of the rocker is constrained by a left stopper 11 and a right stopper 12. Three active forces are acting continuously on the rocker: the force F_r of the recuperative spring, the force F_s of the piston spring and the piston gas force F_p. In addition to these continuous forces, a force of one of the SMA wires is applied to the rocker for a certain amount of time.

The function of the pump described is as follows. Let us assume that the parts of the pump are in the position known as "top dead centre" (TDC), as shown in Figure 1a, and let us consider the moments of the active forces with respect to the revolute joint *O*. In this position, the moment of the force of the recuperative spring is greater than the sum of the moments of the force of the piston spring and the force of the piston gas. This difference between the forces' moments rotates the rocker clockwise while resting on the right stopper 12. This position of the bistable mechanism is called the "right stable position". It coincides with the TDC of the piston. In this right stable position, the suction SMA wire 6 is stretched as much as possible, and the discharge SMA wire 7 is released. During the whole counter-clockwise rotation, the suction stroke of the piston is present. To get the pump out of the right stable position, the suction SMA wire 6 is activated by passing an electric current through it and thus causing its Joule heating and shortening. The emerging in the wire tensile force F_{SMAS} rotates the rocker counter-clockwise. The rocker reaches an intermediate "unstable equilibrium position" in which the total moment of all forces with respect to point *O* is zero. The suction SMA wire's length is determined, so force action stops after passing the rocker's unstable equilibrium position. After this position, the moment of the piston spring force F_s is larger than the sum of moments of the recuperative force F_r and the piston gas force F_p. This turns F_s into a driving force. At the end of the counterclockwise rotation of the rocker, its movement is restricted by the left stopper 11.

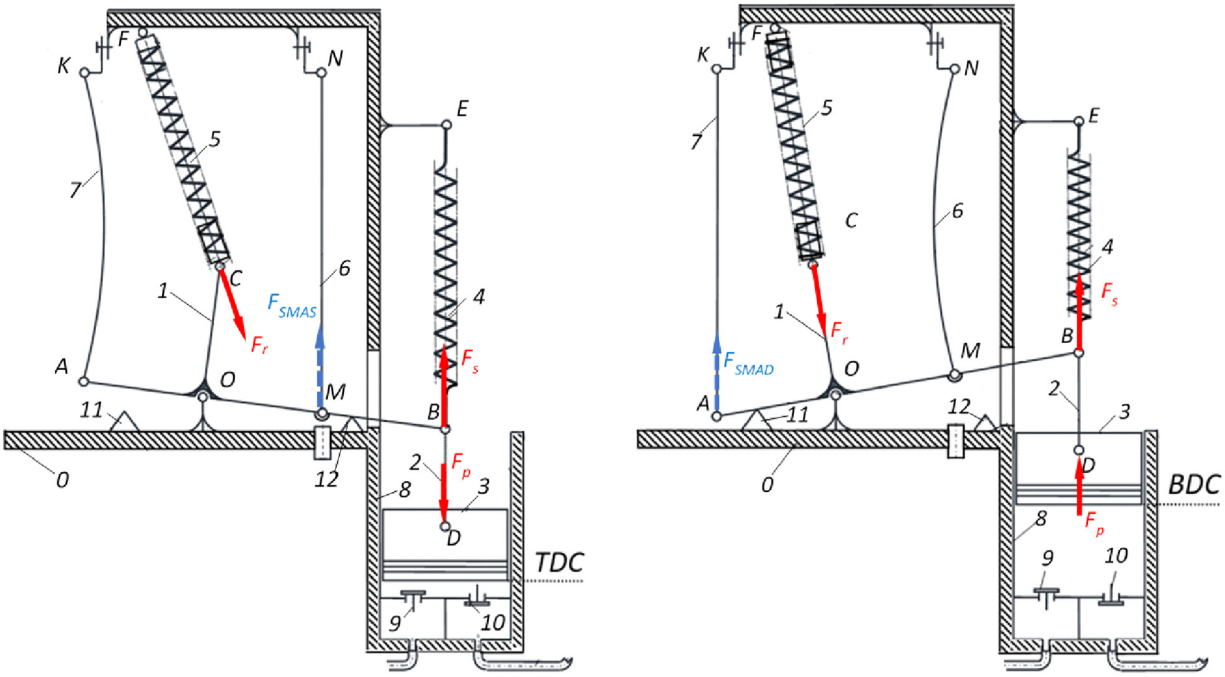

(**a**) (**b**)

Figure 1. Schematic diagram of the pump in: (**a**) Top dead centre (TDC); (**b**) Bottom dead centre (BDC) [31].

The position of the mechanism shown in Figure 1b is the second stable equilibrium position corresponding to the piston's "bottom dead centre" (BDC). The discharge SMA wire 7 pulls the rocker out of this position, rotating it clockwise. This rotation continues until the rocker again passes through the unstable equilibrium position. After that, the force F_r of the recuperative spring drives the rocker until the right stopper restricts its motion. Throughout the clockwise rotation, the piston discharge stroke is carried out.

3. Geometric and Force Relationships for the Pump Suction and Discharge Strokes

Figure 2 depicts a modified schematic diagram of the pump for the position φ of the rocker. To increase the number of possible design options, the kinematic chain of the mechanism compared to Figure 1 is modified. The piston spring 4 is connected to the rocker in point P and the piston and the coupler comprise a single unit 2 consisting of a semi-spherical piston seal and a rigidly connected rod AB.

We would assume that the rocker in Figure 2 rotates counter-clockwise and that the piston then performs a suction stroke. The pressure p acting on the piston as a function of the displacement s of point B is described by the indicator diagram p-s shown in the same figure. The end positions of the rocker are denoted by the dotted lines A_1F_1 and A_2F_2. The stroke of the piston is $h_p = A_1A_2$. A reference coordinate system Oxy with an origin coinciding with the revolute joint O rocker is situated so that its x-axis halves the stroke of the piston h_p.

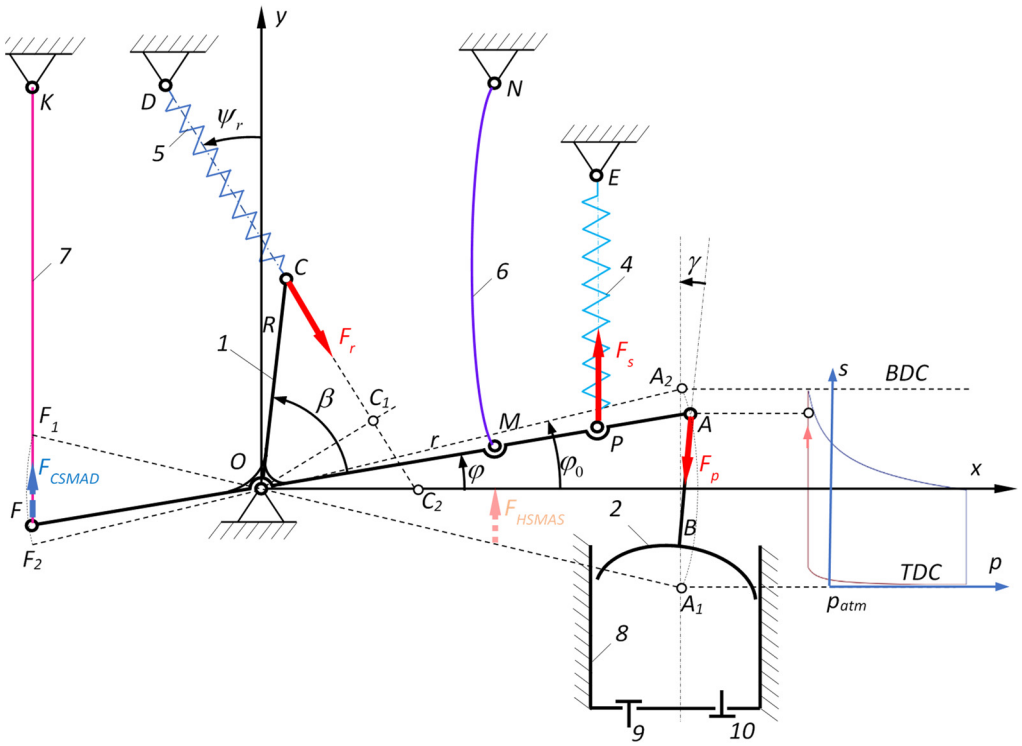

Figure 2. Pump geometry and force layout during the suction stroke.

The end positions of the rocker are symmetrical with respect to the *x*-axis and correspond to the angle φ_0, respectively,—the angle $-\varphi_0$ which is not shown in Figure 2. The following equations represent the position of point C:

$$x_C = R\cos(\varphi+\beta) \tag{1}$$

$$y_C = R\sin(\varphi+\beta) \tag{2}$$

where R is the length of the arm *OC* and $\beta = \sphericalangle AOC$

The working length of the recuperative spring *CD* is denoted by ρ calculated as

$$\rho = CD = \sqrt{\left(x_C - x_D\right)^2 + \left(y_C - y_D\right)^2} \tag{3}$$

Additionally, then the axial force F_r in the recuperative spring is obtained.

$$F_r = \left(l_{R0} - \rho\right)k_r \tag{4}$$

where l_{R0} is the initial nondeformed length of the recuperative spring, and k_r is the stiffness of the recuperative spring.

The moment M_r of the recuperative force with respect to the revolute joint *O* is determined as

$$M_r = -F_r h_r \tag{5}$$

where $h_r = OC_1$ is the distance between the line of action of the recuperative force and point and $OC_1 \perp DC_2$. The negative sign of M_r is due to its clockwise direction.

From the triangle $\triangle OC_1C_2$, after denoting $x_r = OC_2$ and $\psi_r = \sphericalangle C_1OC_2$ the distance h_r is calculated as:

$$h_r = x_r \cos\psi_R \tag{6}$$

where the cosine of the angle between the ordinate and the direction of the recuperative force is

$$\cos\psi_r = \frac{y_D - y_C}{\rho} \tag{7}$$

Additionally, x_r is calculated as:

$$x_r = x_D + y_D \tan\psi_r = x_D + y_D \frac{x_C - x_D}{y_D - x_C} \tag{8}$$

The piston spring force pulls the piston during the suction stroke, and according to the presented schematic diagram and assuming $x_E = r_p \cos\varphi_{in}$ it is expressed by the following equation:

$$F_s = \left[\left(y_E - r_p \sin\varphi\right) - l_{s0}\right] k_s \tag{9}$$

where l_{s0} is the initial length of the piston spring, y_E is the vertical coordinate of point *E*, k_s is the stiffness of the piston spring, also $r_p = OP$.

The moment of the piston spring force with respect to point *O* is:

$$M_s = F_s r_p \cos\varphi \tag{10}$$

The pressure *p* of the gas during the suction stroke creates a piston gas force F_p which depends on the indicator diagram and is presented by the formula

$$F_p = \frac{\pi D^2}{4}(p - p_{atm}) \tag{11}$$

where D is the diameter of the piston, and p_{atm} is the atmospheric pressure.

The angle γ between the vertical axis and the direction of the coupler is:

$$\gamma = \arcsin\frac{r\cos\varphi - x_{B2}}{l} \tag{12}$$

where $x_{B2} = r\sin\varphi_0$ and $l = BD$.

The moment M_p of the piston force F_p with respect to point *O* is calculated using the angle γ as follows:

$$M_p = -F_p r \cos\gamma \tag{13}$$

For the equilibrium of the described moments with respect to point *O*, the following reasoning is appropriate. The two SMA wires apply two kinds of forces to the rocker. The first force is elastic, which arises due to the initial stretching of the wires in their cold martensitic state. The second force drives the pump rocker when it is heated and recovered. For the case in Figure 2, when the piston sucks gas and the rocker rotates counterclockwise, the cold SMA wire force F_{CSMAD} arises when the angle φ becomes bigger than the angle φ_{SD} for which the sum of all moments relative to point *O* is zero. When rotating, the rocker at point *F* stretches the cold SMA wire, then the force is computed using the following equation:

$$F_{CSMAD} = \begin{cases} \dfrac{E_M A_{SD}}{l_{SD}} r_F \left(\varphi_{SD} - \varphi\right) & IF\ \varphi_{in} \geq \varphi \geq \varphi_{SD}\ \ AND\ \ T_{SMA} < A_f \\ 0 & IF - \varphi_{in} \leq \varphi < \varphi_{SD}\ \ AND\ \ T_{SMA} < A_f \end{cases} \tag{14}$$

where E_M is Young's modulus of the SMA wire at a cold martensitic state, A_{SD} and l_{SD} are the cross-section area and the length of the SMA wire FK, T_{SMA} is the SMA wire temperature, A_f is the final austenite temperature of the SMA wire, and $r_F = OF$.

To ensure a longer pump lasting time and reliability, the strain ε_{CSAMD} of the SMA wire should be limited to a value of (2.5 ÷ 3)% [1,32,33]:

$$\varepsilon_{CSAMD} = \Delta l_{SD} / l_{SD} \leq 0.025 \tag{15}$$

where $\Delta l_{SD} = \left(\varphi_{SD} - \varphi_{in}\right) r_F$ is the deformation of the SMA driving wire. To satisfy condition (15) the entire length of the wire can be calculated using the following equation:

$$l_{SD} \geq (\varphi_{SD} - \varphi_{in}) r_F / 0.025 \tag{16}$$

The cross-section A_{SD} of the SMA wire must be calculated at the beginning of the discharge stroke, considering that it is in the high-temperature austenite phase and Young's modulus is about two times larger than at the low-temperature martensite. The moment condition at the beginning of the discharge stroke is written as:

$$M_{HSMAD}\left(-\varphi_{in}\right) = \frac{E_A A_{SD}}{l_{SD}} r_F^2 \left(\varphi_{SD} - \varphi_{in}\right) > M_r\left(-\varphi_{in}\right) + M_s\left(-\varphi_{in}\right) + M_p\left(-\varphi_{in}\right) \tag{17}$$

whence the following formula is derived:

$$A_{SD} > \frac{\left[M_r\left(-\varphi_{in}\right) + M_s\left(-\varphi_{in}\right) + M_p\left(-\varphi_{in}\right)\right] l_{SD}}{E_A r_F^2 \left(\varphi_{SD} - \varphi_{in}\right)} \tag{18}$$

This moment is caused by the rotation of the rocker and one can see it has a potential character because it is a position load. The cold SMA discharge wire force F_{CSMAD} creates a moment M_{CSMAD} with respect to point *O* equal to:

$$M_{CSMAD} = -F_{CSMAD} r_F = -\frac{E_M A_{SD}}{l_{SD}} r_F^2 \left(\varphi_{SD} - \varphi\right) \qquad if\ \varphi > \varphi_{SD} \tag{19}$$

The force F_{HSMAS} of the hot SMA suction wire is controlled and its appearance depends on the instant in which electricity is passed through the wire. For the considered case in Figure 2, this force must act from the beginning of the piston motion when $\varphi = \varphi_{in}$ and is expressed approximately as

$$F_{HSMAS} = \begin{cases} \dfrac{E_A A_{SS}}{l_{SS}} r_M \left(\varphi - \varphi_{in}\right) & if\ \varphi < \varphi_{SS} \\ 0 & if\ \varphi \geq \varphi_{SS} \end{cases} \tag{20}$$

where E_A is Young's modulus for the hot austenitic state, A_{SS} is the cross-section area of the SMA suction wire, l_{SS} is the length of the SMA suction wire, $r_M = OM$. The angle φ_{SS} is the angle in which the current of the hot SMA suction wire is switched off and it must be larger than the angle corresponding to the point of instability.

The length of the wire and the mechanism geometry are chosen so the force F_{HSMAS} becomes zero when $\varphi \geq \varphi_{SS}$. The wire must generate a driving moment M_{HSMAS} which brings the system out of its first stable position:

$$M_{HSMAS} = \begin{cases} F_{HSMAS} r_M = \dfrac{E_A A_{SS}}{l_{SS}} r_M^2 \left(\varphi - \varphi_{in}\right) & if -\varphi_{in} \leq \varphi \leq \varphi_{SS} \\ 0 & if\ \varphi_{in} \geq \varphi > \varphi_{SS} \end{cases} \tag{21}$$

The suction SMA wire becomes cold at the end of the discharge stroke. Then, the rocker rotates clockwise and stretches the suction SMA wire after the angle value $\varphi > \varphi_{SS}$. Furthermore, the electrical current for this wire must be switched off. The force F_{CSMAS} that generates this cold SMA suction wire is expressed as:

$$F_{CSMAS} = \begin{cases} \dfrac{E_M A_{SS}}{l_{SS}} r_M \left(\varphi_{SS} - \varphi\right) & if -\varphi_{in} \leq \varphi < \varphi_{SS} \\ 0 & if\ \varphi_{in} > \varphi \geq \varphi_{SS} \end{cases} \tag{22}$$

where the cross-section area A_{SS} is calculated as:

$$A_{SS} > \frac{\left(M_r\left(\varphi_{in}\right) + M_s\left(\varphi_{in}\right) + M_p\left(\varphi_{in}\right)\right) l_{SD}}{E_A r_M^2 \left(\varphi_{SS} - \varphi_{in}\right)} \tag{23}$$

Additionally, the minimum length of the SMA suction wire l_{SS} is

$$l_{SS} \geq (\varphi_{SS} + \varphi_{in}) r_M / 0.025 \tag{24}$$

The moment of the cold SMA suction wire with respect to point *O* is

$$M_{CSMAS} = \begin{cases} F_{CSMAS} r_M = \dfrac{E_A A_{SS}}{l_{SS}} r_M^2 \left(\varphi - \varphi_{in}\right) & if -\varphi_{in} \leq \varphi \leq \varphi_{SS} \\ 0 & if\ \varphi_{in} \geq \varphi > \varphi_{SS} \end{cases} \tag{25}$$

The balance of the moments determines the three equilibrium positions of the considered bistable mechanism. As clarified above, there are two stable equilibrium positions at the beginning and end of the piston stroke and one unstable position at the middle of the stroke.

For the first stable equilibrium position at the beginning of the stroke, if the hot SMA suction wire force still has not emerged (i.e., $F_{HSMAS} = 0$), the balance of the moments must be negative:

$$\Delta M_1(-\varphi_0) = M_r + M_s + M_{p1} + M_{CSMAS} < 0 \tag{26}$$

In this inequality, the moment created by the cold SMA suction wire must be considered. Although an electrical current does not activate the suction wire, it exerts a moment on the rocker due to its elastic properties in the cold state.

The unstable equilibrium position is determined by the angle φ_{ne}, satisfying the equation:

$$M_r\left(\varphi_{ne}\right) + M_s\left(\varphi_{ne}\right) + M_p\left(\varphi_{ne}\right) = 0 \tag{27}$$

Here, the value of the angle φ_{ne} is constrained by the inequality $-\varphi_0 < \varphi_{ne} < \varphi_0$.

The third equilibrium state is this second stable position at the end of the piston stroke, and it must satisfy the inequality.

$$\Delta M_2(\varphi_0) = M_r + M_s + M_p + M_{CSMAD} > 0 \quad (28)$$

Here, the moment M_{CSMAD} cannot be excluded because it is not a controllable load, and it always appears when $\varphi > \varphi_{SD}$.

The equations for the stable and unstable positions are essential for the kinematic and force synthesis of the pump mechanism. Synthesis cannot be performed without taking into account the reverse stroke of the piston when performing the discharge motion. The discharge stroke starts from the *BDC* and ends in *TDC* position of the piston—see Figure 3. During this stroke, the rocker rotates clockwise, so the driving moment for the suction stroke turns into resistant and vice versa. According to this, for the discharge stroke, the positive moments will be resistant and negative ones will be driving.

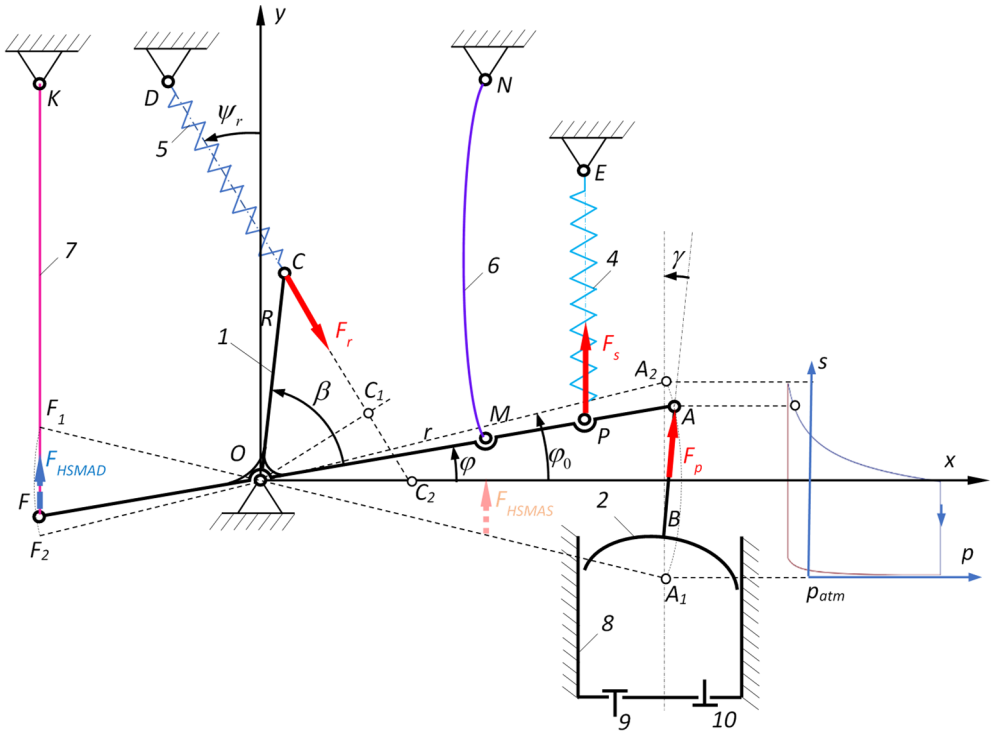

Figure 3. Pump geometry and force layout for the discharge stroke.

4. Numerical Study and Discussions

A series of numerical experiments were carried out to prove the concept for energy recuperation in the studied bistable reciprocating piston pump with a limited stroke. The studies were conducted using the numerical values for the parameters in Table 1.

Table 1. Design parameters for numerical study of the bistable pump with recuperation action.

Parameter Name and Symbol	Numerical Value and Unit
Maximum absolute pressure, p_h	1 MPa
Minimum gas pressure, p_l	50 kPa
Stroke of the piston, h_p	0.016 m
Diameter of the piston, D	0.03 m
Atmospheric pressure, p_{atm}	101,325 Pa
Length of the coupler, l	0.415 m
Length of the arm, r	0.125 m
Vertical coordinate of the point E, y_E	0.1 m

Distance *OC*, *R*	0.065 m
Angle *AOC*, β	75°
Horizontal coordinate of point *D*, x_D	0.025 m
Vertical coordinate of point *D*, y_D	0.1 m
Stiffness of the recuperative spring, k_R	900 kN/m
Stiffness of the piston spring, k_s	20 kN/m
Discharging SMA wire distance, r_F	0.0625 m
Initial coupler angle, φ_{SD}	0.128°
Martensite Young's module of SMA, E_M	21.7 × 10⁹ Pa
Austenite Young's module of SMA, E_A	55.5 × 10⁹ Pa
Suction SMA wire distance, r_M	0.0625 m

With consideration to the balance of the moments (17) with respect to point *O* for the beginning of the suction stroke, the force exerted by the gas on the piston was determined for the maximum absolute pressure p_h and the minimum gas pressure was chosen to be p_l. Figure 4a shows the simplified indicator diagram, presenting the piston's absolute gas pressure *p* as a function of the displacement *s* [34]. More accurate forms of the indicator diagram were presented in [35,36], but the simplified form was used here to avoid complicated outcomes.

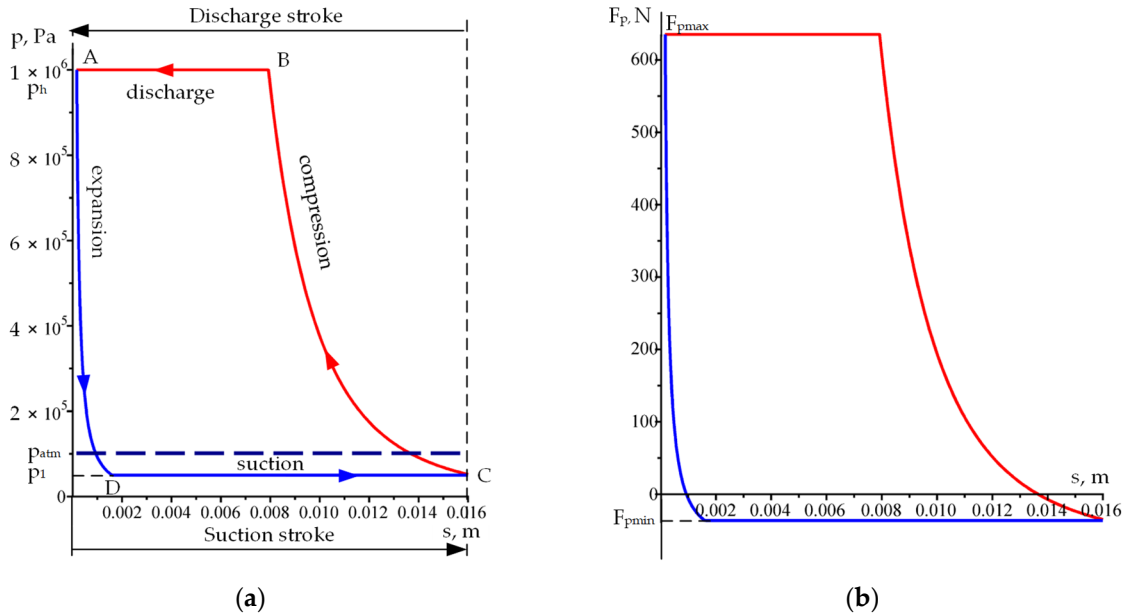

(**a**) (**b**)

Figure 4. The indicator diagram and piston forces: (**a**) The indicator diagram *p*–*s* and atmosphere pressure p_{atm}. (**b**) Diagram of the piston gas force F_p vs. displacement of the piston *s*.

The change of the absolute pressure in the transient intervals (the zones where the pressure changes from maximum to minimum and vice versa) follows the polytropic process described by the following relationship [37]:

$$pV^n = C \tag{29}$$

where *p* and *V* are the gas's pressure and volume, *n* is the polytropic index, and *C* is a constant. Using (29), the transient pressure functions are written as:

$$p_1 = \frac{c_1}{s^{n_1}},\ p_2 = \frac{c_2}{s^{n_2}} \tag{30}$$

where p_1 is the function between the maximum and minimum pressures and p_2 is the function between the minimum and maximum pressures. The polytropic constants were determined using (29) and accepted notations in Figure 4a:

$$c_1 = p_h s_B^{n_1} \tag{31}$$

$$n_1 = \frac{\ln \frac{p_l}{p_h}}{\ln s_B - \ln(h_p + c_l)} \tag{32}$$

$$c_2 = p_h c_l^{n_2} \tag{33}$$

$$n_2 = \frac{\ln \frac{p_l}{p_h}}{\ln s_D - \ln c_l} \tag{34}$$

In the above equations, s_B and s_D are the abscises of the points *B* and *D* (see Figure 4a). Accepting for the stroke of the piston value of h_p, for the clearance $c_l = h_p/100$, for the diameter of the piston *D*, also a value for the atmospheric pressure p_{atm}, the indicator diagram determining the force F_p as a function of the piston displacement *s* is plotted in Figure 4b.

The pump synthesis starts from the load distribution, defined by Equation (13), considering that the piston gas force depends on the differential pressure $p-p_{atm}$. When the piston sucks the gas, the rocker rotates counterclockwise, and thus, the direction of angular velocity is accepted as positive. The moment of the piston force M_p during the suction stroke according to Equation (13) is presented graphically in Figure 5a. The position angle of the rocker is assumed to change in the interval $\varphi \in \left[-\varphi_{in}, \varphi_{in}\right]$, and for its zero position (for $\varphi = 0$), a horizontal disposition of the arms *AO* and *OF* is assumed. The following notations are accepted: for the stroke of the piston h_k, for the length of the coupler *l*, and for the length of the arm *r*. The numerical value of the rocker angle for which the piston is in *BDC* position is $\varphi_{in} = 3.66°$ and is computed using the equation:

$$\varphi_{in} = \arctan \frac{h_p}{2r} \tag{35}$$

Figure 5a shows that at the beginning of the suction stroke during the expansion, the moment of the piston gas is positive, indicating that for a small interval of φ the gas forces generate a positive driving moment. After the expansion, the moment of the piston gas forces becomes entirely negative (resistive) and has a relatively small magnitude.

The moment of the piston spring M_s as a function of the angle φ is shown in Figure 5b. The graph is obtained using the relation $l_{s0} = 0.9\left[y_E - r_p \sin(-\varphi_{in})\right]$. The moment M_r of the recuperative force is presented in Figure 6a calculated using the numerical values shown in Table 1 and $l_{R0} = 1.2\rho_{\max}$, where $\rho_{\max} = \max_{\varphi \in [-\varphi_{in}, \varphi_{in}]} CD$. The resulting moment for the suction stroke is:

$$M_{sum1} = M_{p1} + M_s + M_r \tag{36}$$

Additionally, its graph is shown in Figure 6b. The shaded negative area between the graph line and the *x*-axis shows the potential energy the SMA wire force must overcome. The shaded positive area indicates that in the corresponding interval of change of angle, the recuperative moment will drive the rocker without using the SMA wire. From the graph, one can see that the SMA wire must pull the rocker in the interval $\varphi \in \left[\varphi_{in}, \varphi_{r0}\right]$ and at point φ_{r0} the SMA wire force can be removed.

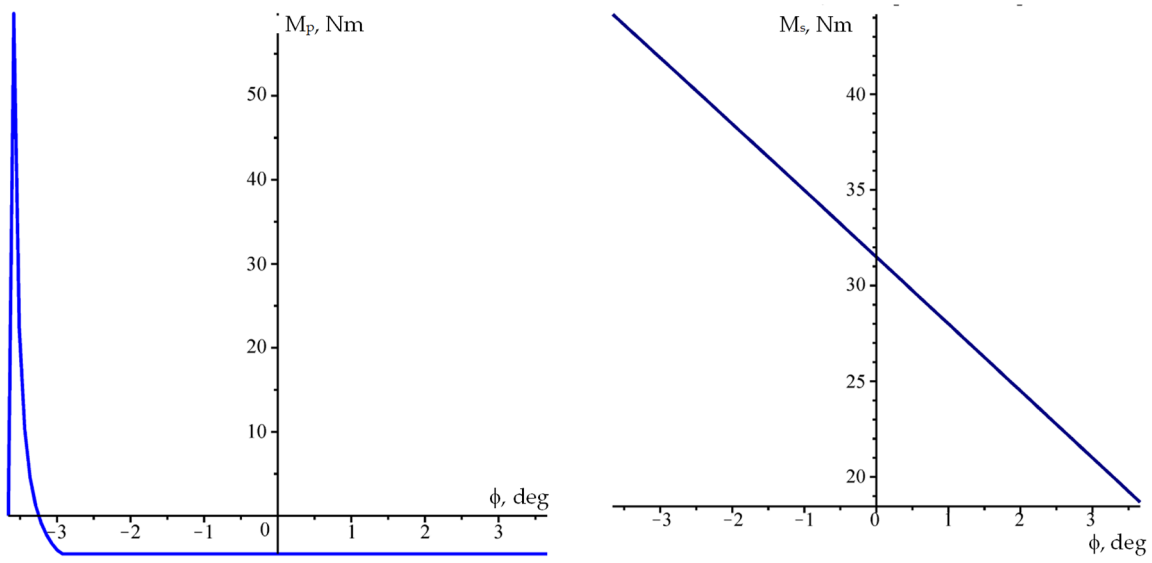

(**a**) (**b**)

Figure 5. Load distribution for the suction stroke: (**a**) The piston force moment M_{p1}; (**b**) Spring force moment M_s.

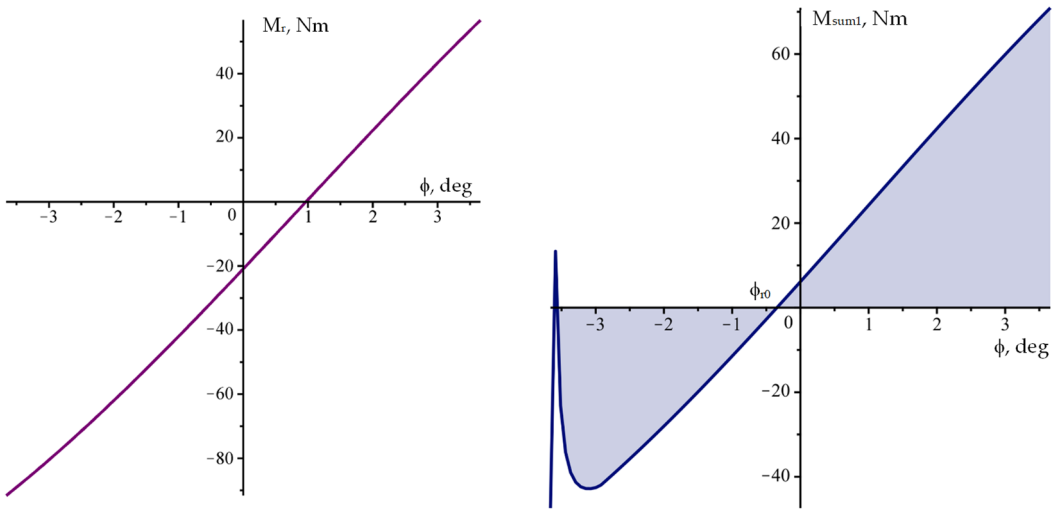

(**a**) (**b**)

Figure 6. The moment distribution for the suction stroke in the interval $\varphi \in \left[-\varphi_{in}, \varphi_{in}\right]$: (**a**) The moment M_r of the recuperative force l; (**b**) The resulting moment M_{sum1}.

During the suction stroke, the rocker rotates from its initial position TDC when $\varphi = \varphi_{in}$ to its final position BDC when $\varphi = -\varphi_{in}$. Figure 7 presents a scaled schematic view of the layout of the synthesized pump mechanism for the two stable positions. As seen in Figure 7a, the distance h (see Figure 2) at the beginning of the stroke is maximal, and the recuperative moment has the maximum absolute value. Because the sign of the moment, in the beginning, is negative and the rocker rotates counterclockwise, the moment of the recuperative spring is resistive. The piston spring is maximally stretched at the initial position, generating a maximal piston spring moment. In Figure 7b, the distance h_r changes its sign, and this is the reason for the positive value of M_r. After the change of the sign, the recuperative moment turns from resistive to driving moment. At *BDC*, the moment of the

piston spring force is minimal because the piston spring has minimal stretching in this position.

For the discharge stroke, the moments of the recuperative force and piston spring force remain the same as shown in Figure 5a,b, respectively. For the discharge stroke, the moment M_{p2} of the gas piston force depends on the indicator diagram (see Figure 4) and is shown in Figure 8a. One can see that at the beginning of the discharge stroke, the moment of the piston force is negative for a small interval of the change of angle φ. This is because the pressure of the gases decreases during the suction stroke. After the value of $\varphi \approx 2.5^0$, the piston force moment becomes positive and resists the motion of the piston. Comparing both piston force moments for the suction and discharge strokes, it is seen that the work performed by the driving forces is considerably bigger during the discharge stroke. This work is proportional to the positive area of the piston force moment graph. The graphs of the three moments M_{p2}, M_s, and M_r are shown in Figure 8b.

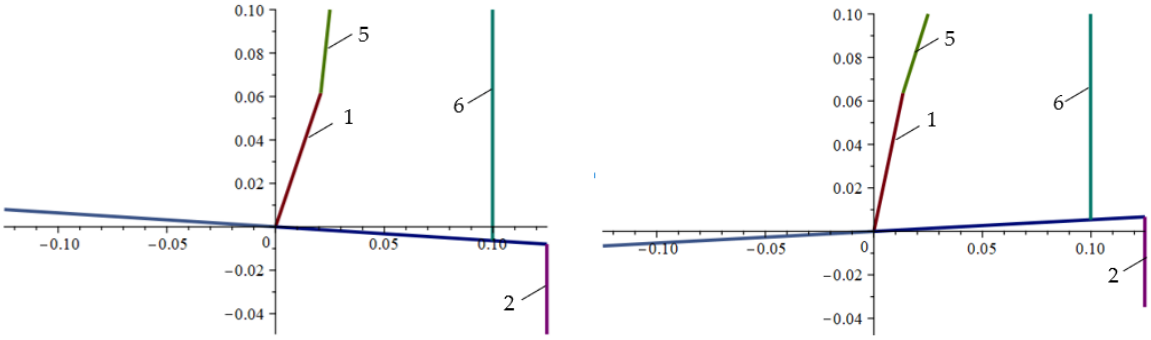

(**a**) (**b**)

Figure 7. A scaled skeleton diagram of the pump: (**a**) Initial TDC position for $\varphi = \varphi_{in}$; (**b**) Final BDC position for $\varphi = -\varphi_{in}$. The labels of the links are as in Figure 2.

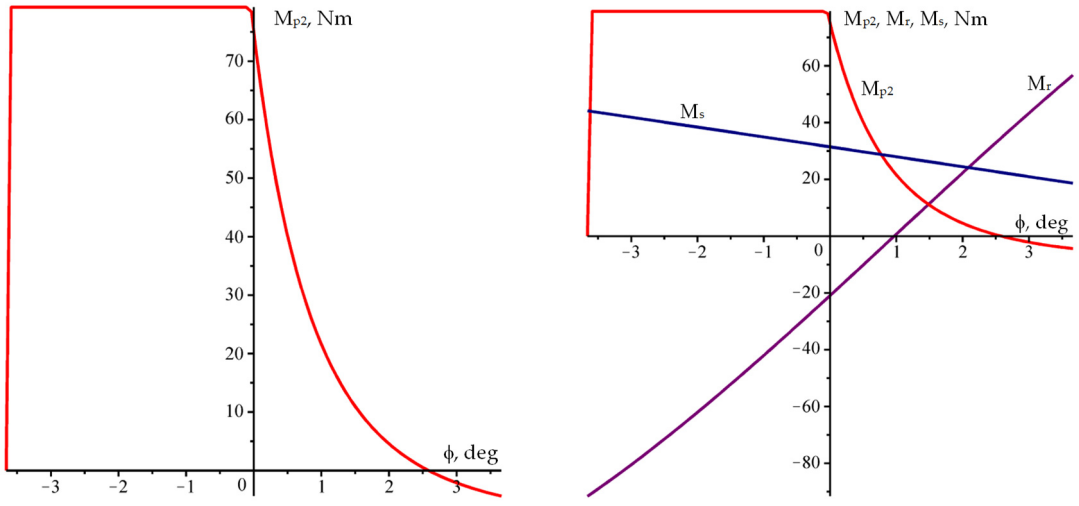

(**a**) (**b**)

Figure 8. Distribution of the moments for discharging stroke: (**a**) The piston force moment M_{p2}. (**b**) The general layout of the piston moment Mp_2, spring moment M_s and recuperative spring moment M_r.

Here, it is essential to highlight that owing to the change of the sign of the rocker angular velocity, the resistive moments would have swapped roles with the driving ones. The graph of the resulting moment for the discharge stroke is shown in Figure 9.

$$M_{sum2} = M_{p2} + M_s + M_r \tag{37}$$

Figure 9 indicates that all other loads are resistive except for one short period at the end of the discharge interval. This contradicts the idea of energy recuperation since the SMA wires must exert forces throughout all intervals to pump the fluid. To avoid this disadvantage, the stiffness of the recuperation spring is changed from $k_R = 900$ kN/m to $k_R = 2500$ kN/m. Using this value, the graphs of the moments for the suction and discharge strokes are obtained and shown in Figure 10a,b, respectively. Figures 11a and 12b show the corresponding total moments for the suction and discharge strokes. The analysis of both graphs shows that at the beginning of both strokes, there is a resistive load, which the SMA wire's forces must overcome. Then, both graphs show areas of loads with positive work, indicating the movement will be on account of the piston or recuperative spring for the suction or discharge stroke, respectively. These two areas of different types of driving forces are evidence of the desired effect of energy recuperation with bistability.

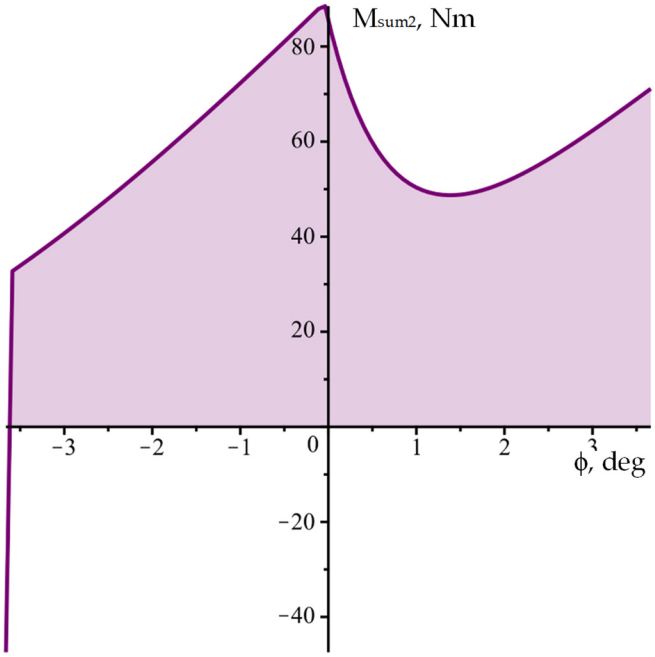

Figure 9. Graph of the resulting moment for the discharge stroke.

To investigate the influence of the SMA wires in their cold state on the loading of the mechanism and on the existence of a point of instability, their action is considered in the model. For the discharge SMA wire, the numerical values shown in Table 1 for the distance r_F, the initial angle φ_{SD}, Young's modules E_M and E_A for martensitic and austenitic states, respectively, are accepted [1,33,38]. According to (16), the discharge SMA wire length is calculated as $l_{SD} = 0.192$ m. Considering (18) and the maximum value of the total moment in Figure 10, a numerical value for the cross-section of the discharge SMA wire is found $A_{SD} = 1.73 \times 10^{-6}$ m^2. The graph of the cold discharge SMA wire is shown in Figure 12a. This behaviour of the moment is possible if the SMA discharge wire is entirely cooled and its entire volume is in the martensitic state.

The graph in Figure 12b shows that the moment of the cold SMA wire, which rotates the rocker during the discharge stroke, counteracts the piston spring. This means that the

cold SMA discharge wire increases the load at the end of the suction stroke. The comparison of graphs in Figures 11a and 12b shows that the cold SMA discharge wire shifts the instability position (P_{IS} point) to the right.

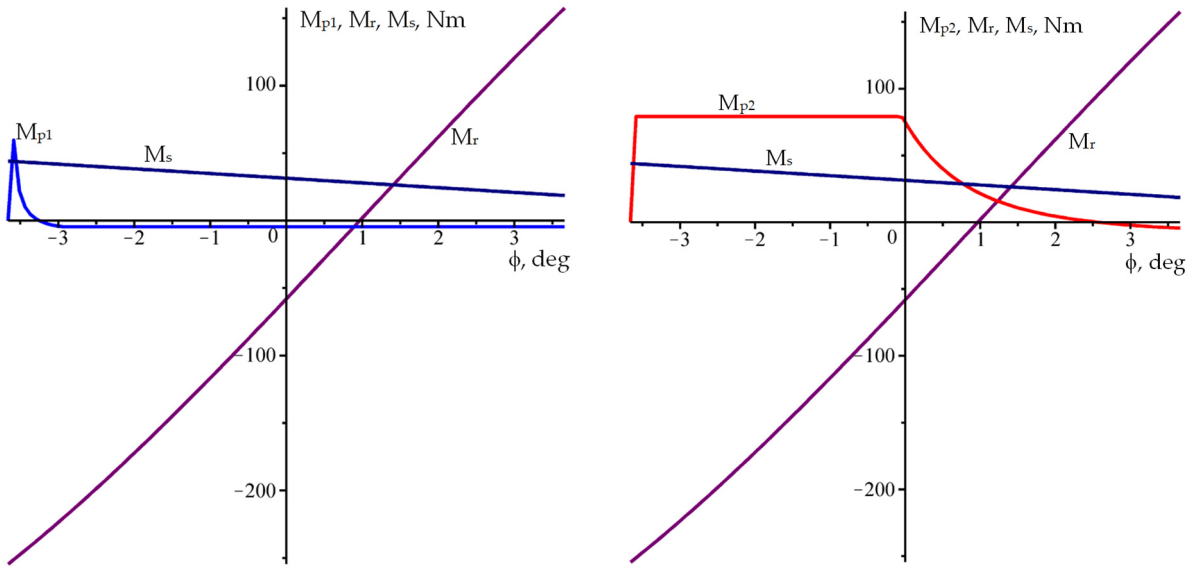

(**a**) (**b**)

Figure 10. Comparative view of the moments for a modified recuperative spring with stiffness $k_R = 2500$ kN/m: (**a**) The moments M_{p1}, M_s and M_r for the discharge stroke. (**b**) The moments M_{p2}, M_s and M_r for the suction stroke.

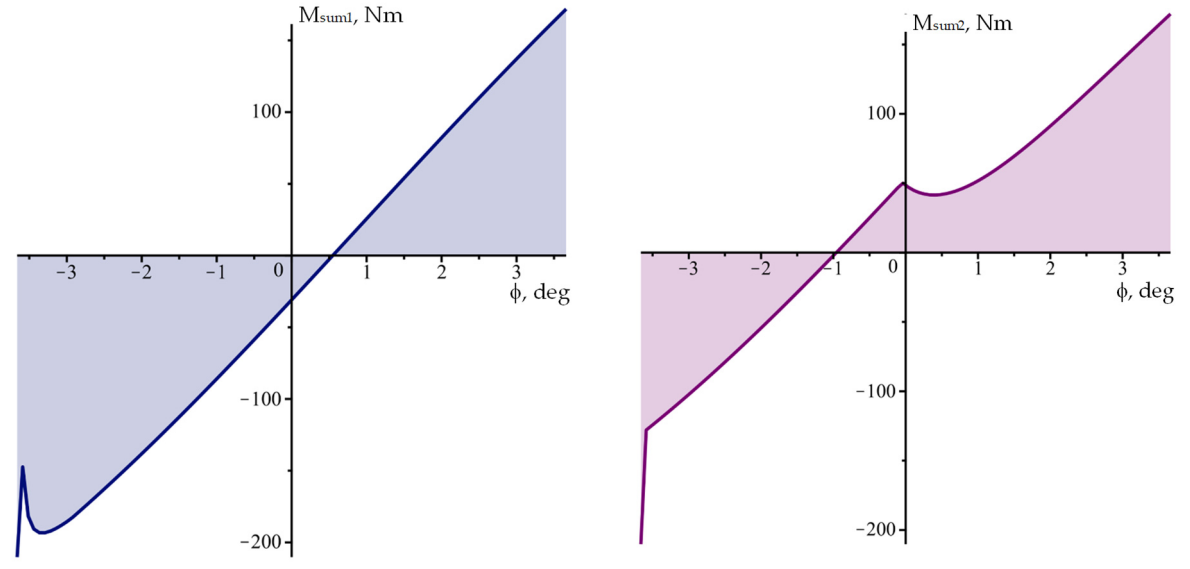

(**a**) (**b**)

Figure 11. The distribution of the resulting moments for a modified recuperative spring with stiffness $k_R = 2500$ kN/m: (**a**) For the discharge stroke. (**b**) For the suction stroke.

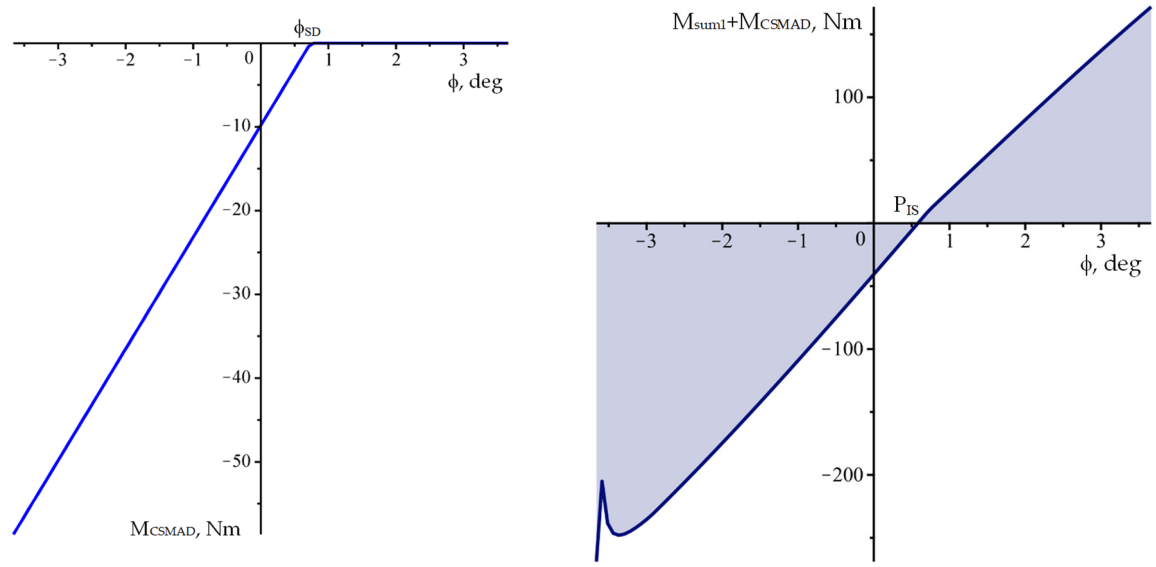

(**a**) (**b**)

Figure 12. The influence of the discharge SMA wire on the moment for the discharge stroke: (**a**) The graph of the cold SMA discharge wire moment. (**b**) The graph of the total moment during the suction stroke considering the moment of the cold SMA.

By choosing r_M = 0.0625 m, φ_{SS} = −0.05 rad and using (23) and (24), the following values for the cross-section area A_{SS} = 1.38 × 10⁶ m², and length l_{SS} = 0.285 m for the cold SMA suction wire are calculated. The computed moment of the cold SMA suction wire is shown in Figure 13a and is added to the moments that act during the suction stroke. The graph of the total moment is shown in Figure 13b. The comparison between Figures 11b and 13b shows that the force of the cold SMA suction wire increases the loading at the beginning of the discharge stroke. The cold SMA suction wire moment shifts the point of instability to the left.

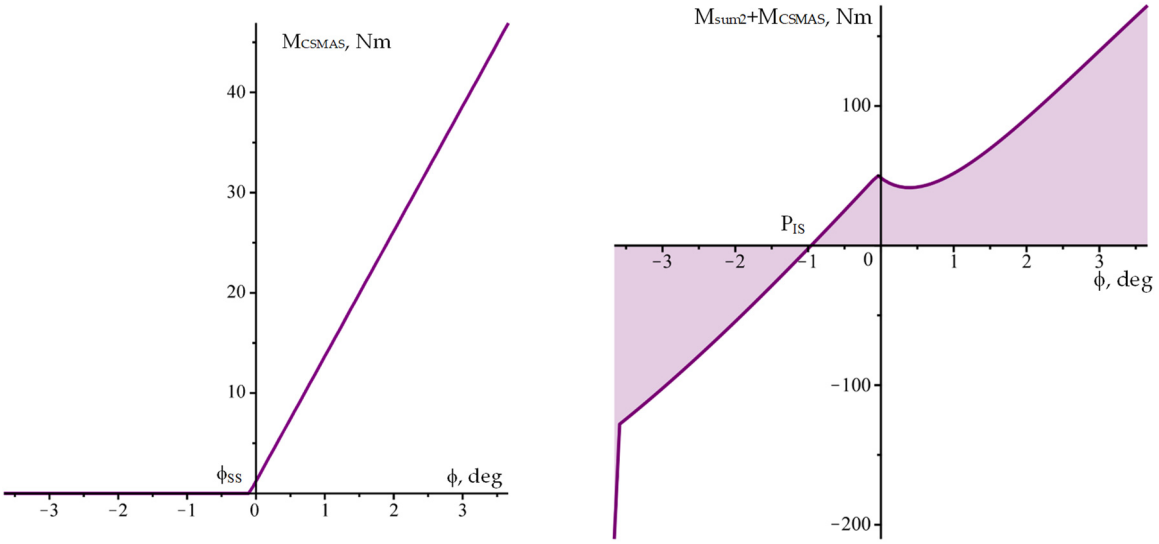

(**a**) (**b**)

Figure 13. The influence of the suction SMA wire on the moment for the suction stroke: (**a**) The graph of the cold SMA suction wire moment. (**b**) The graph of the total moment during the discharge stroke considering the moment of the cold SMA suction wire.

5. Experimental Study

The idea for the bistable pump studied was inspired by the design of a bistable valve patented and experimentally studied by the authors, based on the same principle of operation but different loading of the links [26]. Figure 14a [26] shows a schematic layout of the bistable fluid valve, while Figure 14b shows the picture of the experimental prototype. In Figure 14, the following labels are used: pos.1—rocker, pos.2—lever, pos.3—recuperative spring, pos. 4—SMA wires. The valve is triggered between the open and closed positions on the same principle as the bistable pump—by heating and cooling the SMA wires 4. The movement is assisted by recuperative spring 3 that accumulates the elastic potential energy. For this reason, it can be considered that the results of the valve study can be transferred by analogy to the bistable pump.

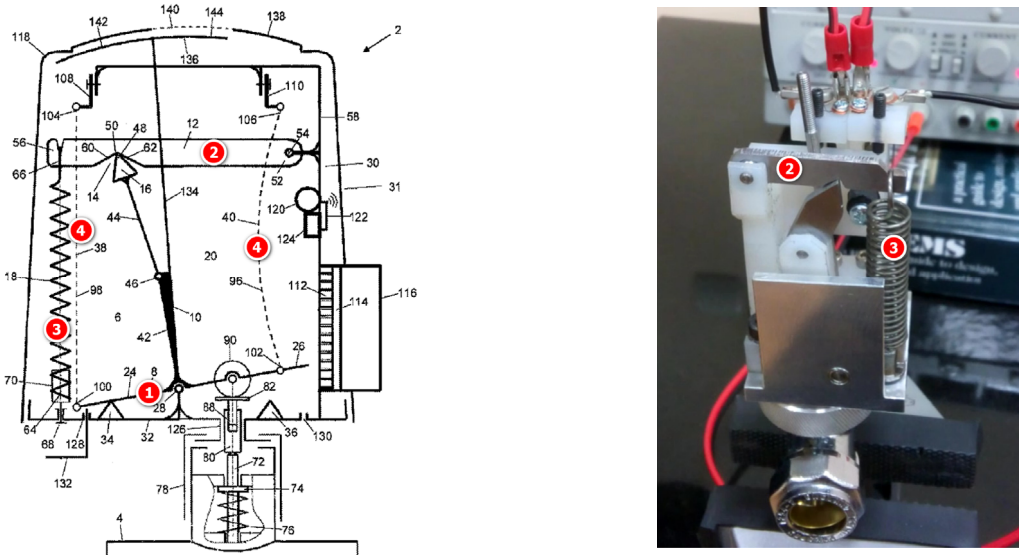

(**a**) (**b**)

Figure 14. SMA actuated fluid valve: (**a**) Schematic layout [26]. (**b**) Physical prototype.

To establish the characteristics of the valve opening and closing process, experimental measurements were performed using a Fastec TS5 high-speed camera with a resolution of 1280 × 1024 and a frame rate of 991 fps. Frames from the high-speed camera are shown in Figures 14 and 15. The frame in Figure 15a shows the time at which the valve closure was initiated, and Figure 15b shows the time at which the valve was fully closed.

From the timer of the camera, it is evident that the closing time was $\Delta t_o = 4.04 - 3.58 = 0.46$ s. If we ignore the transient in the circuit, we can assume, as can be seen from Figure 15, that the current is I = 0.39 A and the voltage is U = 2.6 V. The electric power with which the valve is closed is $P = UI = 0.39 \times 2.6 = 1.01$ W, the energy consumed is $E = P\Delta t_o = 1.01 \times 0.46 = 0.47$ J. Similarly, Figure 16 shows the frames of the initial (Figure 16a,b moments of the valve opening. From the figure, it can be seen that the electrical parameters are I = 0.39, the voltage is U = 2.7 V and the opening time is Δt_c = 6.58 − 6.03 = 0.55 s. Then, by analogous calculations, it is found that the power is 1.05 W and the energy consumed is 0.57 J.

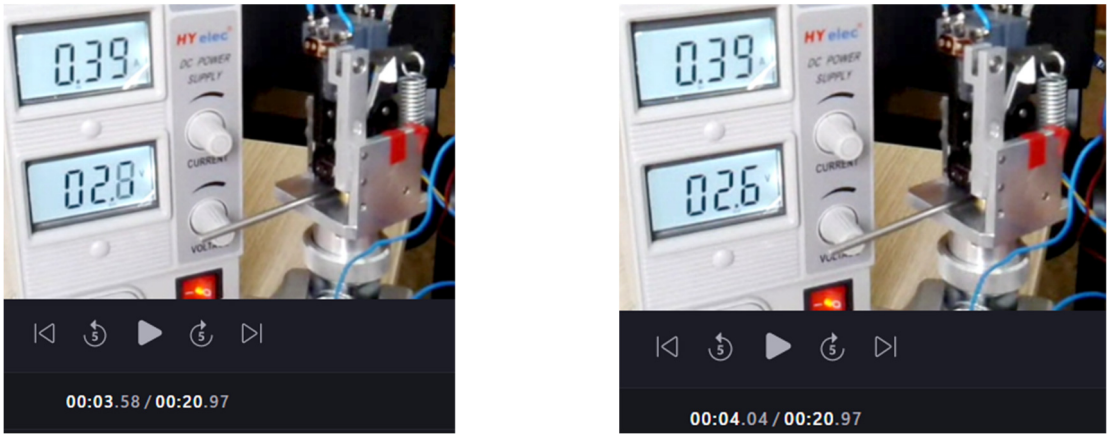

(**a**) (**b**)

Figure 15. Frames corresponding to the valve closing process: (**a**) beginning of the valve closure; (**b**) end of the valve closure.

(**a**) (**b**)

Figure 16. Frames corresponding to the valve opening process: (**a**) beginning of the valve opening; (**b**) end of the valve opening.

In conclusion, it can be said that the on-off power for the bistable valve is about 1 W, the energy consumed is less than 0.6 J, and the frequency of the valve is $f = \left(\Delta t_o + \Delta t_c\right)^{-1} \approx 1$ Hz . This result for the frequency confirms the known disadvantage of the SMA drive, namely the low operating frequency. In interpreting the obtained experimental results, it should be considered that they were achieved without the pump design optimization or optimal control. They show that the energy expended is low because the SMA wires were only switched on at the beginning of the stroke to switch from the bistable position in which the mechanism was positioned. The movement to the next stable position was then carried out by the recuperating springs under the influence of the potential energy stored. Another advantage of the pump concept is that once the SMA wire is heated and the lever system is switched, the second wire can be heated immediately afterwards, and these return the mechanism to its initial position. While one wire heats up, the other has enough time to cool down and this increases the dynamic response of the mechanism. The main challenge here, the cooling of the SMA wires, can be overcome by using more wire with smaller cross sections to increase their surface area and this is expected to reduce the temperature time constant. Furthermore, it is envisaged that in further bistable pump development, the SMA wires will be placed in a low temperature chamber. The experimental investigation of the valve proved that SMA wires could be

used as actuators in similar devices, and the recuperative spring can drive the device moving parts independently during a part of the operating cycle.

6. Conclusions

A new design concept of a bistable reciprocating piston pump with a spring used to recuperate energy was developed. The bistable action of the pump combined with a recuperative spring is controlled by small triggering forces applied at the beginning of the suction and discharge strokes. The triggering forces must act only at the beginning of the strokes; after that, the energy stored in the recuperative spring drives the pump. This is essential in order to reduce energy consumption. Shape Memory Alloy wires create the controlling forces because of their appropriate elastic properties in cold and hot states. One of the main challenges in this pump's design is achieving stable end positions despite the significant non-uniformity of the load in both directions of the piston movement. The condition for the existence of bistability requires two stable end positions and one unstable intermediate position of the pump mechanism. The research findings show that achieving energy recuperation in a bistable reciprocating piston pump with a limited stroke is possible if a correct choice of the geometric and power characteristics is performed.

The benefits of the developed pump design concept compared to conventional pumps are expected to be: (1) To be of higher energy efficiency, as it requires actuation only at the initial moment of the movement, after which the movement is just under the influence of the potential energy accumulated in the springs; (2) more compact design due to the small size of the SMA wire and its high power density; (3) silent operation and impact absorption when the piston stroke ended ; (4) the possibility to control the dynamics of the wire, respectively, of the whole kinematic chain connected to it, with a suitable control system; for example, using the Pulse Width Modulation control principle. The results obtained make it possible to determine the parameters of the SMA wires. In the future, the bistable mechanism's geometric and force synthesis results will be used to optimize the device's energy cost.

Author Contributions: Conceptualization, M.K., T.T. and R.M.; methodology, M.K., K.K. and T.T.; validation, T.T. and R.M.; investigation, M.K., T.T., R.N. and R.M.; resources, T.T. and R.M.; writing—original draft preparation, M.K. and T.T.; writing—review and editing, M.K. and T.T. All authors have read and agreed to the published version of the manuscript.

Funding: This work was supported by the European Regional Development Fund within the Operational Programme "Science and Education for Smart Growth 2014–2020" under the Project CoE "National center of mechatronics and clean technologies "BG05M2OP001-1.001-0008.

Data Availability Statement: Not applicable.

Conflicts of Interest: The authors declare no conflict of interest.

References

1. Lagoudas, D. Shape memory Alloys. In *Modeling and Engineering Applications*; Springer: New York, NY, USA, 2008.
2. Concilio, A.; Antonucci, V.; Auricchio, F.; Lecce, L.; Sacco, E. Shape Memory Alloy Engineering for Aerospace, Structural and Biomedical Applications; Elsevier: Oxford, UK, 2015.
3. Jani, J.; Leary, M.; Subic, A.; Gibson, M. A review of shape memory alloy research, applications and opportunities. *Mater. Des. (1980–2015)* **2014**, *56*, 1078–1113.
4. Meng, L.; Kang, R.; Gan, D.; Chen, G.; Dai, J. A Shape Memory Alloy Driven Crawling Robot Utilizing a Bistable Mechanism. In Proceedings of the ASME 2019 International Design Engineering Technical Conferences & Computers and In-formation in Engineering Conference, IDETC/CIE 2019, Anaheim, CA, USA, 18–21 August 2019. https://doi.org/10.1115/DETC2019-97755.
5. Ishii, H.; Ting, K.-L. SMA actuated compliant bistable mechanisms. *Mechatronics* **2004**, *14*, 421–437. https://doi.org/10.1016/s0957-4158(03)00068-0.
6. Scholtes, D.; Seelecke, S.; Rizzello, G.; Motzki, P. Design of a Compliant Industrial Gripper Driven by a Bistable Shape Memory Alloy Actuator. In Proceedings of the ASME 2020 Conference on Smart Materials, Adaptive Structures and Intelligent Systems.

ASME 2020 Conference on Smart Materials, Adaptive Structures and Intelligent Systems, Virtual, Online, 15 September 2020. V001T04A001.
7. Zimmer, L.; Welsch, F.; Kirsch, S.; Rizzello, G.; Seelecke, S.; Motzki, P. Adaptive Material Handling System Based on Shape Memory Alloy Actuators. In Proceedings of the ASME 2020 Conference on Smart Materials, Adaptive Structures and Intelligent Systems. ASME 2020 Conference on Smart Materials, Adaptive Structures and Intelligent Systems, Virtual, Online, 15 September 2020. V001T04A016.
8. Vetriselvi, V.; Geetha, M.; Dhanalakshmi, K. Design and development of electro mechanical bistable functions using shape memory alloy. In Proceedings of the 2018 8th IEEE India International Conference on Power Electronics (IICPE) 2018, Jaipur, India, 13–15 December 2018. Doi: 10.1109/IICPE.2018.8709540
9. Barth, J.; Kohl, M.; A bistable magnetically enhanced shape memory microactuator with high blocking forces, *Phys. Procedia* **2010**, *10*, 189–196.
10. Kim, H.A.; Betts, D.N.; Salo, A.I.; Bowen, C.R. Shape Memory Alloy–Piezoelectric Active Structures for Reversible Actuation of Bistable Composites. *J. Aircr.* **2010**, *48*, 1265–1268. 10.2514/1.J050100.
11. Reynaerts, D.; Van Brusse, H. Design aspects of shape memory actuators, *Mechatronics* **1998**, *8*, 635–656. ISSN 0957-4158.
12. Wang, T.-M.; Shi, Z.-Y.; Liu, D.; Ma, C.; Zhang, Z.-H. An Accurately Controlled Antagonistic Shape Memory Alloy Actuator with Self-Sensing. *Sensors* **2012**, *12*, 7682–7700. https://doi.org/10.3390/s120607682.
13. Nespoli, A.; Besseghini, S.; Pittaccio, S.; Villa, E.; Viscuso, S. The high potential of shape memory alloys in developing miniature mechanical devices: A review on shape memory alloy mini-actuators, *Sens. Actuators A Phys.* **2009**, *158*, 149–160. ISSN 0924-4247. https://doi.org/10.1016/j.sna.2009.12.020.
14. Wilson, S.A.; Jourdain, R.P.J.; Zhang, Q.; Dorey, R.A.; Chris, R.; Bowen, C.R.; Willander, M.; Wahab, Q.U.; Willander, M.; Alhilli, S.M.; et al. New materials for micro-scale sensors and actuators: An engineering review, *Mater. Sci. Eng. R Rep.* **2007**, *56*, 1–129. ISSN 0927-796X. https://doi.org/10.1016/j.mser.2007.03.001.
15. Grant, D.; Hayward, V. Variable structure control of shape memory alloy actuators. *IEEE Control. Syst. Mag.* **1997**, *17*, 80–88. https://doi.org/10.1109/37.588180.
16. Villoslada, A.; Escudero, N.; Martín, F.; Flores, A.; Rivera, C.; Collado, M.; Moreno, L. Position control of a shape memory alloy actuator using a four-term bilinear PID controller. *Sens. Actuator A Phys.* **2015**, *236*, 257–272.
17. Garner, L.J.; Wilson, L.N.; Lagoudas, D.C.; Rediniotis, O.K. Development of a shape memory alloy actuated biomimetic vehicle. *Smart Mater. Struct.* **2000**, *5*, 673–683.
18. Huber, J.E.; Fleck, N.A.; Ashby, M.F. The Selection of Mechanical Actuators Based on Performance Indices. *Proc. R. Soc. Lond. A* **1997**, *453*, 2185–2205.
19. Cai, W.; Meng, X.L.; Zhao, L.C. Recent development of TiNi-based shape memory alloys. *Curr. Opin. Solid State Mater. Sci.* **2005**, *9*, 296–302. https://doi.org/10.1016/j.cossms.2006.07.002.
20. Zhang, J.; Wu, Z.; Zhang, C.; Hao, L.; Nie, R.; Qiu, J. Nonlinear dynamics of shape memory alloys actuated bistable beams. *Smart Mater. Struct.* **2019**, *28*, 055009.
21. Thomas, S.; Almanza, M.; Civet, Y.; Perriard, Y. Actuation Displacement Analysis of a Self-Switching Shape Memory Alloy Buckled Beam. In Proceedings of the 2018 21st International Conference on Electrical Machines and Systems (ICEMS), Jeju-do, Korea, 7–10 October 2018. https://doi.org/10.23919/icems.2018.8549122.
22. Zirbel, S.A.; Tolman, K.A.; Trease, B.P.; Howell, L.L. Bistable Mechanisms for Space Applications. *PLoS ONE* **2016**, *11*, e0168218. https://doi.org/10.1371/journal.pone.0168218.
23. Alvarez, R.; Sirdey, P. Bistable Valve. US8540208B2, 27 June 2006.
24. Leinung, A; Wyen, S.; Schnittger, K. Electrically Actuated Bistable Valve. DE102011114070A1, 28 March 2013.
25. Todorov, T.; Mitrev, R.; Penev, I. Force analysis and kinematic optimization of a fluid valve driven by shape memory alloys, *Rep. Mech. Eng.* **2020**, *1*, 61–76. https://doi.org/10.31181/rme200101061t.
26. Kostov, M.S.; Todorov, T.S.; Milkov, M.J.; Penev, I.R. Bistable Valve Actuator. GB 2558616 A, Ap. No: 1700422.7, 18 July 2018.
27. Hiroyuki, K.; Kazuyuki, H.; Kihara, I. Bistable Pump and Hydraulic Device. Japan Patent JP4052808B2, 27 February 2008.
28. Massie, P. Sealed Pump and Drive Therefor. US3754154A, 21 August 1973.
29. Ericson, P.L. Flex-Actuated Bistable Dome Pump. United States patent US6132187A, 17 October 1999.
30. Anyszewski, J. Bistable Compressor Head. Poland Patenent PL130996B1, 29 September 1984.
31. Kostov, M.S.; T. Todorov, T.S. A Bistable Compressor Driven with Shape Memory Alloys for Refrigerator. UK Patent Application GB2207547.7, 2022, Pending.
32. Lexcellent, C. *Shape-Memory Alloys Handbook*; ISTE Ltd.: London, UK; John Wiley & Sons: Hoboken, NJ,USA, 2013; pp. 1–359.
33. Dynalloy, Inc. Available online: http://www.dynalloy.com/ (accessed on 10 September 2022).
34. Potter, M.; Somerton, C. *Thermodynamics for Engineers*, 4th ed.; McGraw-Hill Education: New York, NY, USA, 2020; p. 188.
35. Hollingsworth, J.; Phillippi, G.; Hinchliff, M.; Kulhanek, C.; Rimpel, A.; Maywald, F. Reciprocating Compressors. *Compress. Mach. Oil Gas* **2019**, *5*, 167–252. https://doi.org/10.1016/b978-0-12-814683-5.00005-5.
36. Ninković, D.; Taranović, D.; Milojević, S.; Pesic, R. Modelling Valve Dynamics And Flow in Reciprocating Compressors. In Proceedings of the International Congress Motor Vehicles & Motors, Kragujevac, Serbia, 3–5 October 3 2012; pp. 113-125, ISBN 978-86-86663-91-7.
37. Cengel, Y.; Boles, M.; Kanoglu, M. *Thermodynamics: An Engineering Approach*, 9th ed.; McGraw-Hill Education: New York, NY, USA, 2019; p. 166.

38. Mitrev, R.; Todorov, T. A Case Study of Experimental Evaluation of the Parameters of Shape Memory Alloy Wires. *AIP Conf. Proc.* **2022**, *2449*, 060010. https://doi.org/10.1063/5.0091153.